iScience

CellPress

Article

A Membrane-Bound Biosensor Visualizes Shear Stress-Induced Inhomogeneous Alteration of Cell Membrane Tension

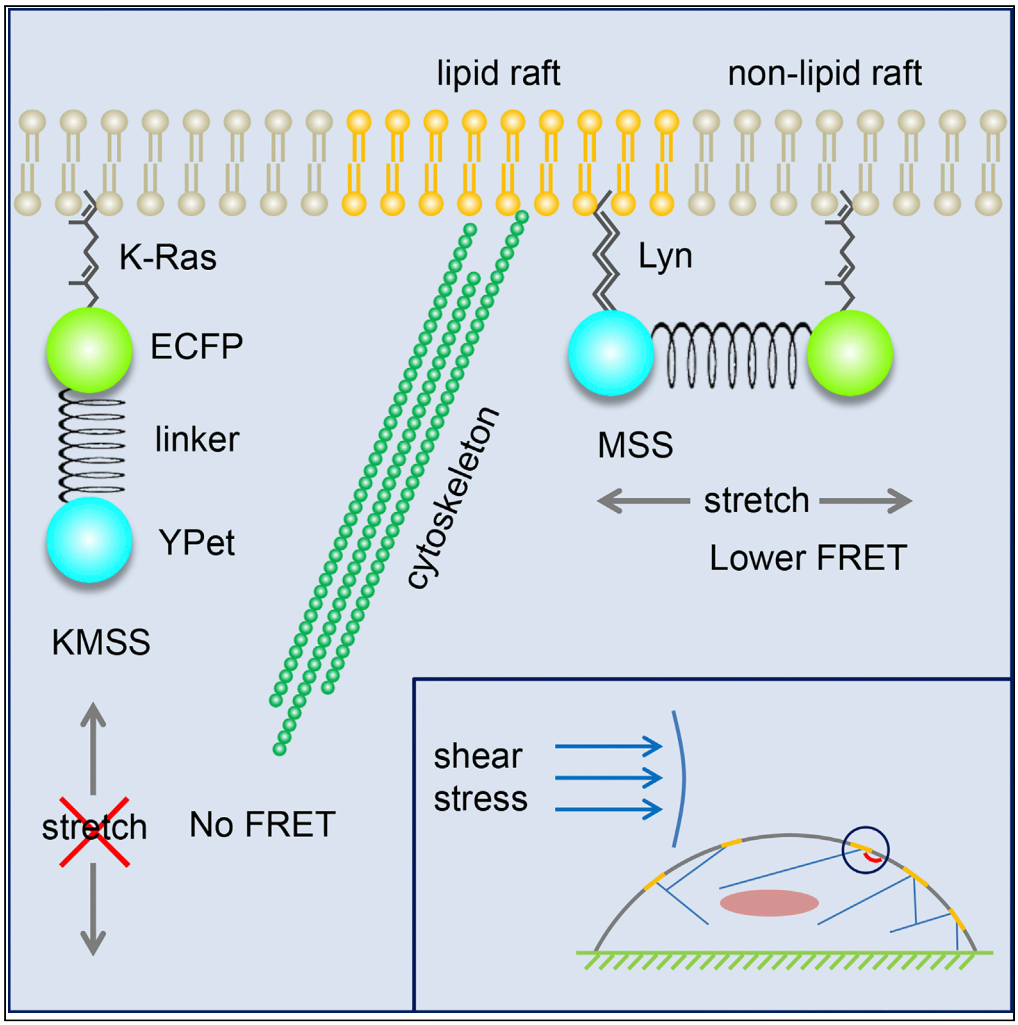

Wang Li, Xinlei Yu, Fei Xie, ..., Aziz ur Rehman Aziz, Xiaoling Liao, Bo Liu

lbo@dlut.edu.cn

HIGHLIGHTS

A FRET-based biosensor (named MSS) is developed to study cell membrane tension

MSS is a beneficial tool to visualize the distribution of membrane tension

Membrane tension is inhomogeneous in response to shear stress

Membrane tension does not display polar distribution during mechanotransduction

Li et al., iScience 7, 180–190
September 28, 2018
https://doi.org/10.1016/j.isci.2018.09.002

iScience

CellPress

Article

A Membrane-Bound Biosensor Visualizes Shear Stress-Induced Inhomogeneous Alteration of Cell Membrane Tension

Wang Li,[1] Xinlei Yu,[1] Fei Xie,[1] Baohong Zhang,[1] Shuai Shao,[1] Chunyang Geng,[1] Aziz ur Rehman Aziz,[1] Xiaoling Liao,[2] and Bo Liu[1,3,*]

SUMMARY

Cell membrane is the first medium from where a cell senses and responds to external stress stimuli. Exploring the tension changes in cell membrane will help us to understand intracellular force transmission. Here, a biosensor (named MSS) based on fluorescence resonance energy transfer is developed to visualize cell membrane tension. Validity of the biosensor is first verified for the detection of cell membrane tension. Results show a shear stress-induced heterogeneous distribution of membrane tension with the biosensor, which is strengthened by the disruption of microfilaments or enhancement of membrane fluidity, but weakened by the reduction of membrane fluidity or disruption of microtubules. These findings suggest that the MSS biosensor is a beneficial tool to visualize the changes and distribution of cell membrane tension. Besides, cell membrane tension does not display obvious polar distribution, indicating that cellular polarity changes do not first occur on the cell membrane during mechanical transmission.

INTRODUCTION

It is well observed that external mechanical stimulus can be transmitted or transduced into intracellular biological signal to regulate cell alignment (Goldfinger et al., 2008), deformation (Pfafferott et al., 1985), differentiation (Altman et al., 2002), and some other cellular functions (Liu et al., 2010). However, the information about detailed signal pathway is limited. At present, it is extensively believed that mechanical stress signal acts on the cell membrane, which activates membrane proteins such as sensitive ion channels, G-protein-coupled receptors, and focal adhesions kinases (Boycott et al., 2013; Chachisvilis et al., 2006; Liu et al., 2014). Consequently, they further activate intracellular signaling chain and regulate gene expression as well as protein synthesis. This could explain the major phenomena of mechanotransduction. However, it has been reported that a rapid (<300 ms) activation of Rac was induced by the stress at cell periphery but there was no Rac activation within 30 s when it was stimulated by platelet-derived growth factor (Poh et al., 2009). Besides, cells display a lot of polar changes upon shear stress stimuli including Cdc42-dependent polarization of microtubule system (microtubule-organizing center) (Tzima et al., 2003; McCue et al., 2006) and different activation levels of Src or focal adhesion kinase at upstream and downstream sites (Liu et al., 2014). These cellular polarized changes may result from the asymmetric distribution of stress during transmission via cell membrane, cytoskeleton, or other signal proteins.

As a barrier of the whole cell, cell membrane is the first medium of mechanotransduction to sense extracellular stress. The induced alteration of membrane tension is likely to be an association between cellular polarized changes and stress distribution. In some neural cells, membrane tension also takes part in regulating vesicle trafficking and driving fusion pore expansion (Apodaca, 2002; Kozlov and Chernomordik, 2015). Studies have reported that high membrane tension activates exocytosis, whereas low membrane tension activates endocytosis (Gauthier et al., 2009). In addition, tension of cell membrane has been shown to regulate many cell behaviors, including cell motility (Gauthier et al., 2011), polarization (Houk et al., 2012), spreading (Raucher and Sheetz, 2000), and membrane repair (Togo et al., 2000). However, how the membrane tension changes in response to external stress remains unclear due to the lack of appropriate tension sensors. Membrane tension is composed of in-plane tension in the lipid bilayer and tension from membrane-cytoskeleton adhesion (Keren, 2011). In recent years, some methods have been developed gradually to measure membrane-associated tension. One way is by using micropipette aspiration, which sucks the cellular surface into a micropipette to form a hemispheric protrusion and thus calculates

[1]School of Biomedical Engineering, Dalian University of Technology, Liaoning IC Technology Key Lab, Dalian 116024, China

[2]Biomaterials and Live Cell Imaging Institute, Chongqing University of Science and Technology, Chongqing 400030, China

[3]Lead Contact

*Correspondence: lbo@dlut.edu.cn

https://doi.org/10.1016/j.isci.2018.09.002

the tension by taking advantage of Laplace's law (Hochmuth, 2000). This technique supplies information about the overall tension of the cell, so it is not appropriate for measuring membrane tension only (Tinevez et al., 2009). Tether pulling is another way to measure membrane tension by pulling membrane tethers from the plasma membrane with the help of optical or magnetic tweezers (Diz-Munoz et al., 2013). The tether force measured by this approach is contributed by in-plane tension, a component of membrane tension, and cytoskeleton attachment to some extent (Lafaurie-Janvore et al., 2013; Dai and Sheetz, 1999). Recently, a new technology based on fluorescence resonance energy transfer (FRET) has been developed to evaluate tension across proteins in focal adhesions that gives a complex distribution of tension within individual focal adhesion (Grashoff et al., 2010; Morimatsu et al., 2013). Such a method could provide the spatial and temporal dynamics of tension visually in living cells in an invasive way.

In the current project, a membrane-bound FRET-based tension sensor (named MSS) is constructed to visualize the dynamics of membrane tension in HeLa cells under applied laminar shear stress of 0.5 (low shear stress), 2 (intermediate shear stress), and 4 Pa (high shear stress) (Mitchell and King, 2013). Cell membrane tension is found to be positively related to cell membrane fluidity but not to the magnitude of shear stress. In addition, shear stress-induced membrane tension depends on the cooperation between cytoskeleton components, although it is mainly maintained by microtubules.

RESULTS

MSS Biosensor Can Visualize Membrane Tension

MSS is a membrane-bound tension sensor, including a tension sensor module and two anchoring proteins, which are linked with lipid molecules in lipid raft and non-lipid raft regions through Lyn and K-Ras kinases, respectively. The tension sensor module comprises an elastic spider silk protein inserted between two fluorescence proteins, enhanced cyan fluorescence protein (ECFP) and yellow fluorescent protein for energy transfer (YPet) (Figure 1A). With this sensor, tension changes can be transformed into FRET efficiency changes of these two fluorescence proteins. The control probe, KMSS, is a head-less mutant whose amino terminal disassociates in the cytoplasm, whereas only the carboxyl terminal anchors on the membrane (Figure 1B). Therefore, no tension could be applied to the KMSS mutant. The FRET ratio of HeLa cells expressing MSS shows no changes over time under static condition (Video S1), demonstrating the stability of the sensor in a living cell. To further check these tension sensors' effects, the osmotic pressure of culture medium is changed artificially. HeLa cells expressing KMSS are exposed to hypertonic solution (0.05 g/mL, sucrose) or hypotonic solution (adding 3 times volume of H_2O into culture medium) separately, but the FRET efficiency remains almost unchanged from the baseline ($p > 0.05$; Figures 1C and 1D), indicating that KMSS is inert to the changes of membrane tension. In contrast, the FRET ratio of HeLa cells expressing MSS achieves a clear higher level in hypertonic solution, whereas it decreases significantly from the baseline in hypotonic solution after 15 min ($p < 0.05$; Figure 1E), demonstrating that MSS is significantly affected and that it is sensitive to the changes of membrane tension induced by osmotic pressure.

Furthermore, when the cells expressing MSS are exposed to hypertonic solution (0.025 g/mL, sucrose) after a hypotonic stimulus (adding 2 times volume of H_2O into culture medium) for 10 min, the FRET ratio reverses immediately, even though it decreases slowly in the beginning (Figure S1A; Video S2). On the contrary, the FRET ratio increases from the start but later decreases slowly when the cells expressing MSS are exposed to hypertonic solution (0.05 g/mL, sucrose) for 10 min first and then to hypotonic stimulus (adding the same volume of H_2O into the culture medium) (Figure S1B). These results suggest that the response of this biosensor to the changes in membrane tension is reversible, whereby it will react quickly if the membrane tension changes in the opposite direction.

In addition, the FRET ratio of MSS increases linearly when cells are exposed to 0.025, 0.5, and 0.075 g/mL sucrose solution (Figure S1C). On the contrary, the ratio decreases linearly after reducing the osmotic pressure of culture medium by adding 1, 2, 3, or 4 times volume of H_2O separately (Figure S1D). Results indicate a linear relationship between the response of MSS biosensor and the changes in membrane tension induced by osmotic pressure in current experiments. Therefore, MSS could be applied to visualize the changes and distribution of membrane tension with good sensitivity, reversibility, and linearity.

Shear Stress Changes Membrane Tension

To check the effects of different shear stresses on cell membrane tension, HeLa cells expressing MSS are exposed to shear stress of 0.5 (MSS-0.5 group), 2 (MSS-2 group), and 4 Pa (MSS-4 group) for 15 min. The group of HeLa cells transfected with KMSS, with shear stress of 2 Pa, serves as control. Results show that

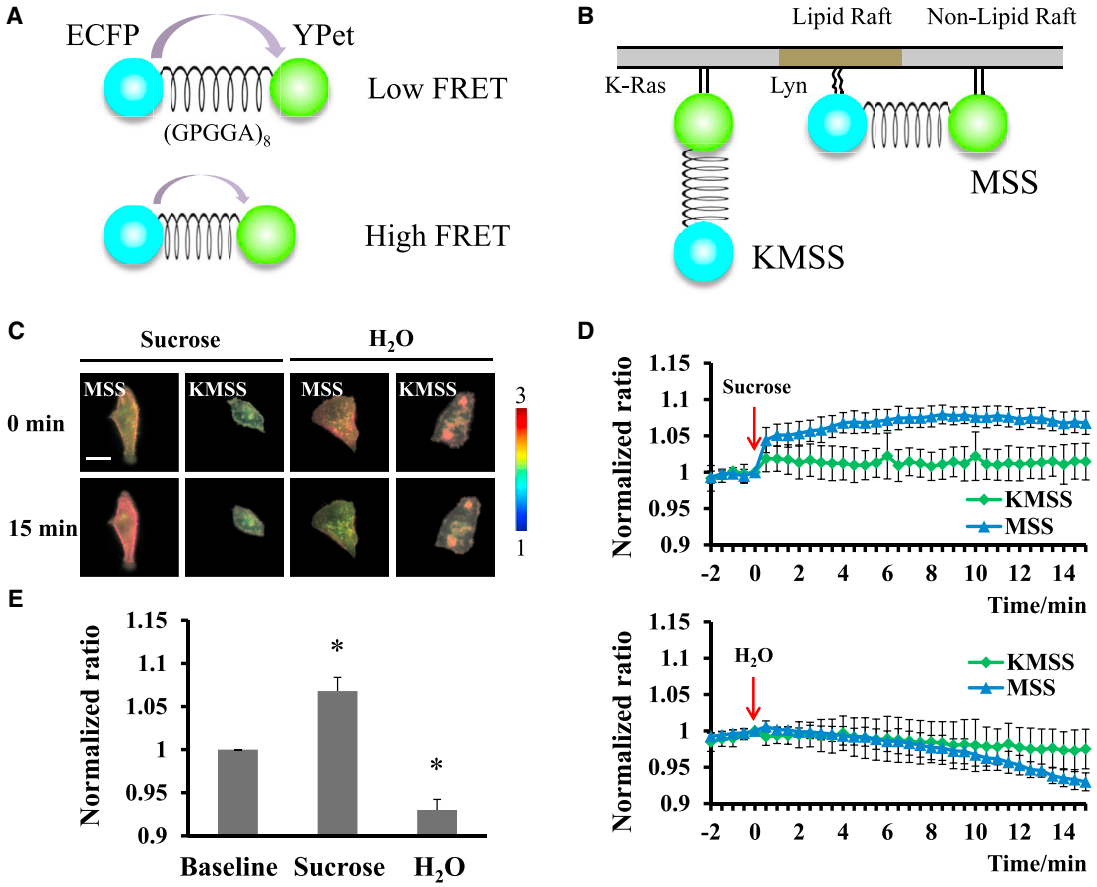

Figure 1. MSS Plasmid Could Visualize the Changes of Membrane Tension

(A) Tension sensor module contains a linker sequence $(GPGGA)_8$ inserted into two fluorescent proteins. When force extends the elastic linker, FRET efficiency decreases, otherwise it increases.

(B) MSS sensor consists of tension sensor module and membrane-bound sequences Lyn and K-Ras. KMSS is a Head-less control sensor of MSS.

(C and D) (C) The representative YPet/ECFP emission ratio images and (D) their average time courses of FRET biosensors in HeLa cells after exposure to hypertonic (MSS, n = 10; KMSS, n = 11) and hypotonic solutions (MSS, n = 7; KMSS, n = 12), respectively.

(E) Average normalized YPet/ECFP emission ratio of KMSS at 0 min (baseline), MSS at 15 min in hypertonic solution (sucrose) and MSS at 15 min in hypotonic solution (H_2O). *$p < 0.05$ significantly different from baseline. All error bars represent SEM.

Scale bar, 20 μm. See also Figure S1.

the FRET ratio of MSS decreases obviously in response to shear tress, whereas that of the control group remains unchanged basically (Figures 2A and 2B). In addition, when the cells are exposed to shear stress, the FRET ratio of MSS decreases sharply within 30 s and then decreases slowly with time whatever be the magnitude of shear stress. Strangely, these are coincident changes of FRET ratio under shear stress of 0.5 and 4 Pa, both of which are lower than the change of FRET ratio under stress of 2 Pa (Figures 2B and 2C), suggesting that membrane tension is not positively related to the magnitude of shear stress.

Further analyses show that cells display a heterogeneous distribution of FRET ratio with the lowest in the middle part, whereas the highest in upstream and downstream parts initially. This distribution manner remains unchanged over time and is not affected by low or high shear stress (Figures 3A and 3B; Videos S3, S4, and S5). By fitting the FRET ratio in different regions of a cell at 0 and 15 min with Extreme equation (Tables S1 and S2), it is found that after its exposure to shear stress, the minimal FRET ratio at 15 min (named min value) decreases, and that 2 Pa induces a significantly larger min value than the other two groups ($p < 0.05$; Figure 3C). However, the position of min value shows a tendency of moving toward downstream as the shear stress ranges from 0.5 to 4 Pa (Figure S2). Furthermore, upstream variation range (UVR) and downstream variation range (DVR) become smaller under shear stress application, especially for 0.5 and 4 Pa, although there is no significant difference between UVR and DVR in spite of the magnitude of shear stress

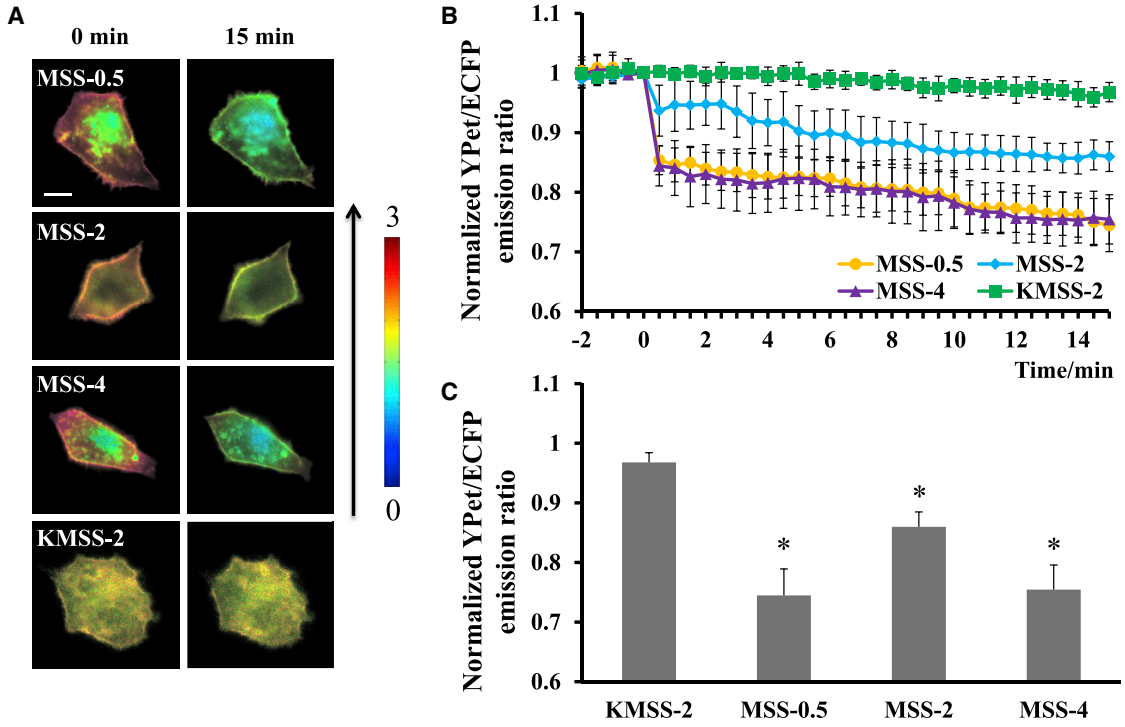

Figure 2. The Overall Changes of Membrane Tension under Different Shear Stresses

(A and B) (A) The representative YPet/ECFP emission ratio images and (B) their average time courses of MSS in HeLa cells after exposure to the shear stress of 0.5 (n = 13), 2 (n = 14), and 4 Pa (n = 11) and KMSS in HeLa cells (served as control) after exposure to the shear stress of 2 Pa (n = 9).

(C) Average normalized YPet/ECFP emission ratio of FRET biosensors at 15 min under different shear stresses. *$p < 0.05$ significantly different from control. All error bars represent SEM.

Scale bar, 10 μm.

(Figure 3D). These results suggest that shear stress can enlarge membrane tension but plays only a gentle role in its uneven distribution.

Cell Membrane Fluidity Regulates Membrane Tension

Cell membrane fluidity is reported to display polarity upon shear stress application (Butler et al., 2002). To check whether the cell membrane fluidity participates in the regulation of membrane tension induced by shear stress, HeLa cells expressing MSS are pretreated with 0.1 mmol/L of cholesterol (Cho) for 3 hr or 45 mmol/L benzyl alcohol (BA) for 15 min to reduce or enhance the fluidity of cell membrane, respectively (Butler et al., 2002). Cells transfected with MSS plasmid under shear stress of 2 Pa, namely, the MSS-2 group, serves as a control group. Upon the stimulus of 2 Pa, BA treatment decreases the FRET ratio sharply, whereas Cho decreases it slowly, although both treatments show a decreasing trend in the FRET ratio (Figures 4A and 4B; Videos S6 and S7). At 15 min, BA treatment leads to a significant lower FRET ratio but Cho leads to a significant higher FRET ratio compared with the control group ($p < 0.05$; Figure 4C). These results demonstrate that cell membrane fluidity affects the alteration of membrane tension induced by shear stress, and higher membrane tension is associated with higher cell membrane fluidity.

Initially, FRET ratio is low in the whole cell after BA or Cho applications, especially under Cho treatment. After exposure to shear stress, the ratio decreases in all regions of the cell (Figure 5A). However, the smallest ratio (at 15 min) is still located in the middle part of the cell (Figure 5B). From the fitting curve, it can be obtained that BA treatment significantly decreases the min value, whereas Cho plays an opposite role ($p < 0.05$; Figure 5C; Tables S1 and S2), but neither of the above treatments changes the position of the min value (Figure S2). Besides, either UVR or DVR is drastically decreased by BA treatment but not by Cho. UVR has no significant difference with DVR whether under BA or Cho application (Figure 5D). These results indicate that cell membrane fluidity plays a significant role in adjusting the distribution of membrane

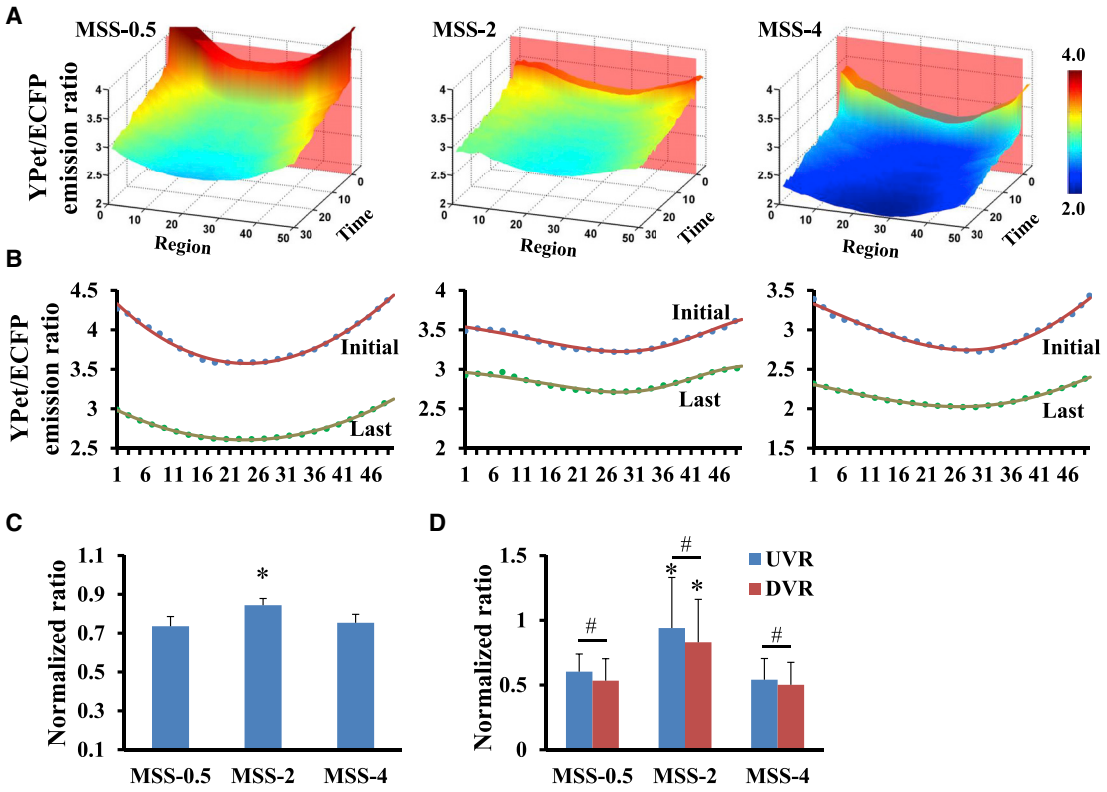

Figure 3. Shear Stress Changes Membrane Tension

(A and B) (A) YPet/ECFP emission ratio of different cellular regions in timescale and (B) the fitting curve (points for sample data and solid lines for fitting) at 0 and 15 min under shear stress of 0.5, 2, or 4 Pa.

(C and D) (C) Comparisons of normalized minimum YPet/ECFP emission ratio and (D) normalized upstream variation range and downstream variation range between different shear stress groups at 15 min *$p < 0.05$ compared with 0.5 Pa group. #$p > 0.25$ between groups of UVR and DVR. All error bars represent SEM.

See also Figures S2 and S3 and Tables S1 and S2.

tension induced by shear stress. They also suggest that enhanced cell membrane fluidity can help to homogenize cellular membrane tension.

Cytoskeleton Regulates Membrane Tension

Studies show that cytoskeleton binds with cell membrane directly and takes part in the process of sensing external stress and mediating mechanical force transduction (Choi and Helmke, 2008; Davies, 2009; Alenghat and Ingber, 2002; Raucher et al., 2000). Therefore, it is tested whether cytoskeleton plays any role in the regulation of membrane tension induced by shear stress. HeLa cells expressing MSS are pretreated with 1 μg/mL of cytochalasin D (CytoD) for 30 min or 5 μg/mL of nocodazole (Noco) for 15 min to destroy actin filaments or microtubules, respectively (Kim et al., 2012; Zaal et al., 2011). It is observed that CytoD decreases FRET ratio significantly, whereas Noco strangely increases the ratio to a higher level compared with the control group (MSS-2 group) ($p < 0.05$; Figure 6; Videos S8 and S9). When HeLa cells expressing MSS are pretreated with 1 μg/mL of myosin light-chain kinase (MLCK) inhibitor, ML7, for 1 hr to suppress the contraction but keep the structure of microfilament intact (Liu et al., 2011), the FRET ratio decreases obviously but is slightly higher than that obtained from CytoD treatment, although the tendency is similar to that of CytoD ($p < 0.05$; Figure 6; Video S10). These results indicate that both microfilaments and microtubules are necessary for maintaining cellular membrane tension.

Furthermore, cells pretreated with CytoD or ML7, but not with Noco, show an obviously decreased ratio in all cellular regions upon shear stress application, and all of them have similar distributions of membrane tension (Figure 7A). It can be seen clearly from the fitting curve that shear stress decreases the min value

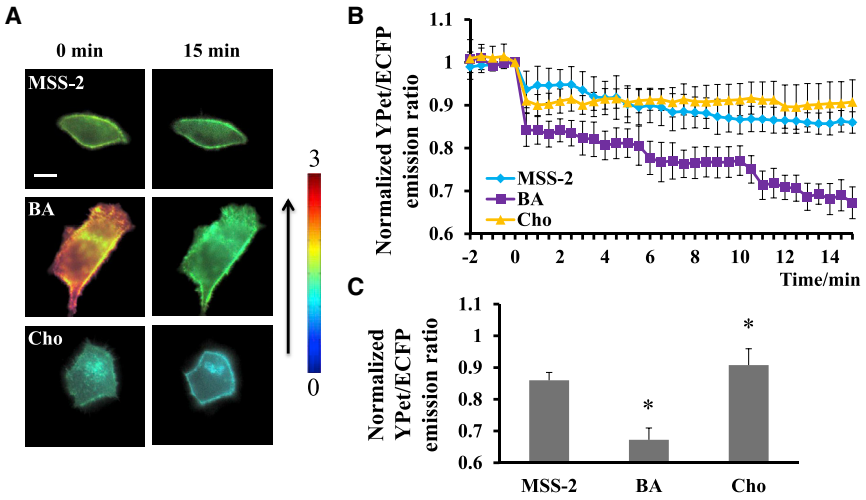

Figure 4. The Overall Changes of Membrane Tension under Different Cell Membrane Fluidities

(A and B) (A) The representative YPet/ECFP emission ratio images and (B) their average time courses of MSS in HeLa cells pretreated for 15 min with 45 mmol/L BA (n = 10) or 3 hr with 0.1 mmol/L of Cho (n = 11) under shear stress of 2 Pa.

(C) Average normalized YPet/ECFP emission ratio of FRET biosensors at 15 min under different cell membrane fluidities.

*$p < 0.05$ significantly different from 2 Pa group. All error bars represent SEM.

Scale bar, 10 μm.

after the cytoskeleton is destroyed, but not obviously under microtubule disruption (Figures 7B and 7C; Tables S1 and S2). Moreover, the position of min value remains almost unchanged under any component disruption of cytoskeleton (Figure S2). Further comparison reveals that UVR has no significant difference compared with the control group after the cytoskeleton disruption, whereas DVR is found different under Noco treatment ($p < 0.05$; Figure 7D). These results suggest that the maintenance of membrane tension depends on the structure and contractility of cytoskeleton, and that the cytoskeleton is supposed to have little effect on the heterogeneous distribution of membrane tension. In addition, there is still no significant difference between UVR and DVR under any kind of treatment (Figure 7D).

DISCUSSION

Many techniques have been used for measuring cell mechanics, including elastic substrates, bendable micropost array, atomic force microscopy, and optical and magnetic tweezers (Xie et al., 2017; Guo et al., 2014). However, these methods have difficulties in detecting intracellular mechanical force. Recently, FRET-based biosensors have been widely used in life sciences field owing to their high temporal and spatial resolution, although only a few studies have applied FRET technology to the research of stress transfer within cells. A tension sensor was reported to be inserted into vinculin protein to study the dynamics of focal adhesion with piconewton sensitivity (Grashoff et al., 2010; Freikamp et al., 2017). This genetically encoded biosensor provides methods to measure intracellular stress, but it is constructed by insertion of the tension sensor into a specific protein, which may affect the function of endogenous protein. Later, a FRET biosensor was developed to describe the tension across membrane receptor, epidermal growth factor receptor (Stabley et al., 2011). Similarly, another group has applied their biosensors to integrin proteins, which has allowed us to visualize the distribution of tensions within individual focal adhesions (Morimatsu et al., 2013). These non-genetically encoded biosensors are developed by linking the tension sensor to the membrane proteins that are usually not part of the endogenous proteins (Liu et al., 2017). They are located outside of the cells so that these biosensors can describe the stress transmission toward intracellular region in a non-invasive manner. In the current project, this membrane-bound biosensor is constructed by extending the two terminals of tension sensor with two different anchor proteins, Lyn and K-Ras, and the tension changes on cell membrane, not a protein, was measured with this biosensor since it was supposed to be the first step of intracellular stress transmission. FRET efficiency decreases under membrane tension because of the larger distances between two fluorophores induced by tension. Results confirm that the MSS biosensor is sensitive to the changes of membrane tension and that this response is reversible as well as linear with the changes in the membrane tension. Furthermore, after in-depth analysis of the relationship

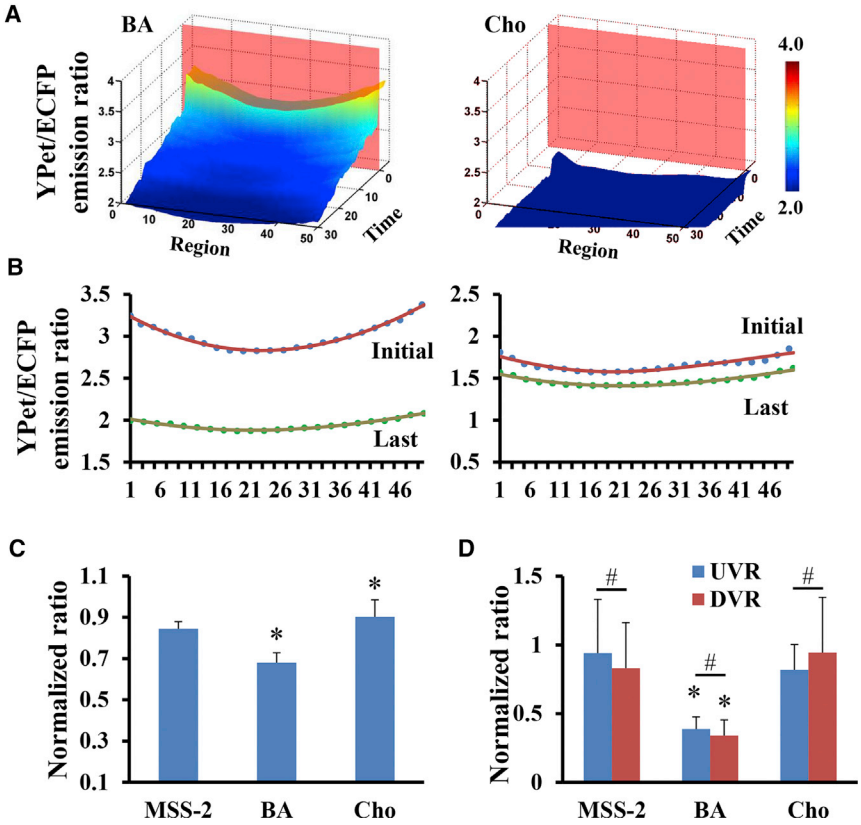

Figure 5. High Cell Membrane Fluidity Enlarges Membrane Tension

(A and B) (A) YPet/ECFP emission ratio of different cellular regions in timescale and (B) the fitting curve (points for sample data and solid lines for fitting) at 0 and 15 min for cells pretreated for 15 min with 45 mmol/L BA or 3 hr with 0.1 mmol/L of Cho under shear stress of 2 Pa.

(C and D) (C) Comparisons of normalized minimum YPet/ECFP emission ratio and (D) normalized upstream variation range and downstream variation range between different membrane fluidities group at 15 min *$p < 0.05$ compared with 2 Pa group. #$p > 0.3$ between groups of UVR and DVR. All error bars represent SEM.

See also Figures S2 and S3 and Tables S1 and S2.

between the FRET-proportional value and the actual stress magnitude by theoretical calculation in current research (Figure S3), it is revealed by the MSS biosensor that membrane tension ranges from 0 to 2 pN under shear stress application, which has the same order of magnitude as in previous reports (Lieber et al., 2013). Therefore, this genetically designed tension sensor can be applied to visualize membrane tension and study the detailed changes of tension on cell membrane with piconewton sensitivity, which provides a powerful tool to explore cellular mechanical transmission.

Current results show that shear stress causes an obvious heterogeneous distribution of membrane tension, which is the highest in the midstream but lower at upstream and downstream. Either cell membrane fluidity or cytoskeleton has slight effects on this uneven distribution. However, shear stress can strengthen membrane tension, although it is not directly proportional to the amplitude of shear stress. Strangely, low shear stress induces higher membrane tension than that under intermediate shear stress. It has been reported that cortical actin cytoskeleton forms a meshwork at the cell periphery just beneath the plasma membrane while some actin filaments and microtubules are connected directly with lipid rafts in cell membrane (Allen et al., 2007; Hall, 1998; Viola and Gupta, 2007). In response to low shear stress, a quick reduction of RhoA activity is observed corresponding to a decrease in the formation of actin stress fibers in C28/I2 chondrocytes (Wan et al., 2013). Therefore, membrane tension is increased under low shear stress as less stress fibers reduce restriction on the mobility of lipid molecules, while lipid rafts are still confined by microtubules. Consistently, cell membrane also exhibits higher tension compared with that under intermediate shear stress after destroying the structure or contractility of microfilaments artificially. Different from the

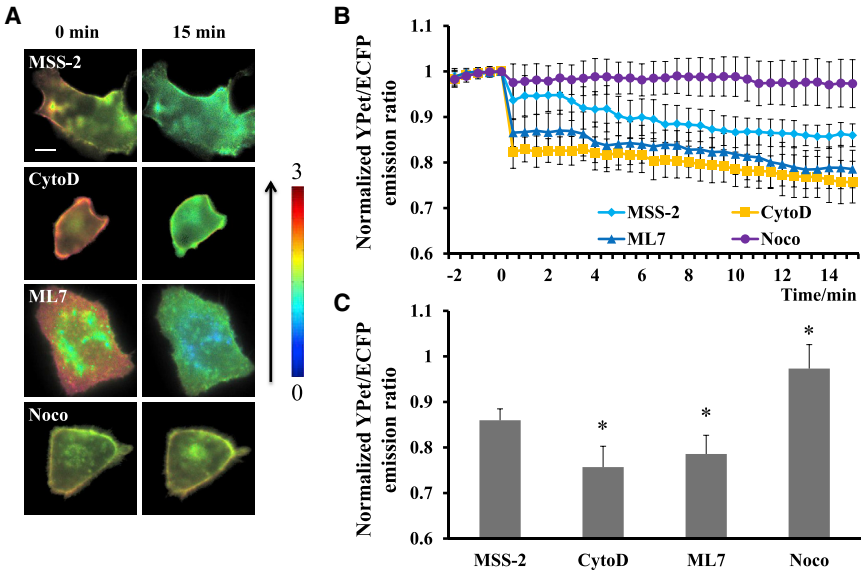

Figure 6. The Overall Changes of Membrane Tension under Different Disruptions of Cytoskeleton

(A and B) (A) The representative YPet/ECFP emission ratio images and (B) their average time courses of MSS in HeLa cells pretreated for 30 min with 1 μg/mL of CytoD (n = 13), 15 min with 5 μg/mL Noco (n = 18), or 1 hr with 1 μg/ml ML-7 (n = 10) under shear stress of 2 Pa.

(C) Average normalized YPet/ECFP emission ratio of MSS at 15 min with different pretreatments. *$p < 0.05$ significantly different from control. All error bars represent SEM.

Scale bar, 10 μm.

nonlinear association between membrane tension and shear stress, the position of maximum membrane tension moves toward downstream with increasing shear stress. It has been reported with computational finite element modeling techniques that cell deformation induced by fluid shear stress (0.6 Pa) is the largest in the midstream part (McGarry et al., 2005). Higher shear stress may push the position of maximum membrane tension to the downstream since it has larger tangential effects on the middle part of cell membrane.

It has been reported that the overall cell membrane fluidity increases upon higher laminar shear stress application (Butler et al., 2001). Present results indicate that high shear stress can increase membrane tension significantly and quickly, which may be due to the increased cell membrane fluidity since enhancement of cell membrane fluidity can accelerate this process. This swift change of membrane tension is consistent with an immediate (5 s) significant increase in membrane fluidity under shear stress application (Butler et al., 2001). It seems that higher membrane fluidity promotes the relative movement of phospholipid molecules and thus stretches cell membrane and leads to higher membrane tension. This has been verified in the current experiments by enhancing or reducing the cell membrane fluidity. The results also show that higher membrane fluidity helps to homogenize membrane tension. Consistently, high shear stress has also reduced the variation ranges of membrane tension in both upstream and downstream significantly.

The generation of membrane tension has been reported to have a close association with integrated actin cytoskeleton (Cramer, 1999). Recently, an investigation about ezrin, a major cross-linker of the membrane-cytoskeleton interface, has shown that membrane tension is decreased after reducing ezrin activity (Rouven Bruckner et al., 2015). Membrane mechanics could also be altered by the presence of actin shell, which seems to lead to a larger friction coefficient and restrict lipid mobility (Guevorkian et al., 2015). Current experiments find that disruption of microtubules decreases membrane tension, whereas actin disruption increases the tension. Microtubules may enhance the membrane tension by anchoring lipid rafts in the membrane, but if microtubules are destroyed, there will be little limitations on lipid rafts, which lead to a reduction of membrane tension. According to the above discussion, actin disassembly and the inhibition of its contractility enable more freedom for lipid molecules' mobility but less for lipid raft mobility, which results in increased membrane tension. These findings demonstrate that any of the cytoskeleton components as well as their contractility contributes to membrane tension. However, the local distribution of

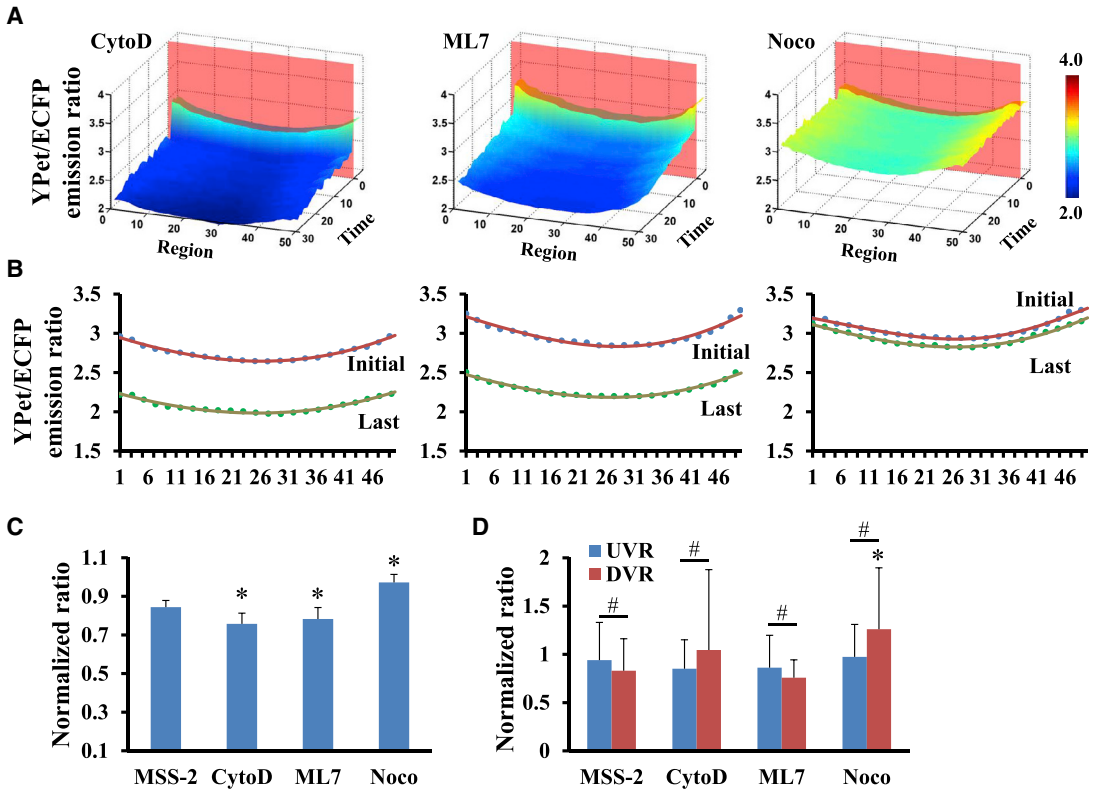

Figure 7. The Membrane Tension Depends on Not Only Microtubules but Also Actin Filaments

(A and B) (A) YPet/ECFP emission ratio of different cellular regions in timescale and (B) the fitting curve (points for sample data and solid lines for fitting) at 0 and 15 min for cells pretreated for 30 min with 1 μg/mL of CytoD, 15 min with 5 μg/mL Noco, or 1 hr with 1 μg/ml ML-7 under shear stress of 2 Pa. (C and D) (C) Comparisons of normalized minimum YPet/ECFP emission ratio and (D) normalized upstream variation range and downstream variation range at 15 min with different pretreatments. *$p < 0.05$ compared with 2 Pa group. #$p > 0.11$ between groups of UVR and DVR. All error bars represent SEM. See also Figures S2 and S3 and Tables S1 and S2.

membrane tension is nearly not affected by cytoskeleton, since UVR and DVR remain almost unchanged after being pretreated with cytoskeletal-disrupting agents. Some interfaces have been reported to be formed between membrane and cytoskeletal proteins, known as plasma membrane skeleton (Sechi and Wehland, 2000; Smith et al., 2017). Some other membrane-associated proteins like supervillin, myosin, talin, and G-protein-coupled receptor also connect cell membrane to actin filaments or microtubules (Allen et al., 2007; Chichili and Rodgers, 2009). These interactions may also contribute to maintaining membrane tension along with its local distribution. Moreover, microtubule disruption seems to eliminate the tension changes in all cellular regions under shear stress application, suggesting that microtubules play a main role in maintaining membrane tension. This is supported by a previous report that cellular morphology usually depends on the interaction of microtubules with plasma membrane (Kuchnir Fygenson et al., 1997).

Shear stress can induce a lot of cellular polarity changes, like polarized Rac activation at cellular downstream (Shao et al., 2017). During this process, external stress signal is transmitted to target molecules step by step. However, which step first reveals polar changes remains unclear. The present results observe that membrane tension does not display obvious polar distribution, suggesting that cell membrane only plays a role in transmitting stress intracellularly. It has been reported that local stress could activate Src in 0.3 s at remote cytoplasmic sites, which depends on the tension across cytoskeleton (Na et al., 2008). Microtubules are reorganized and stress fibers become thicker and longer after shear stress stimuli (Galbraith et al., 1998). Therefore, cytoskeleton, which is considered as the subsequent pathway of stress transmission after plasma membrane, will display polar distribution of tension probably. This is supported by a previous report that actin filaments could enable the establishment of a polarized distribution by breaking symmetry condition, whereas microtubules maintain the stability of the polarized organization

(Li and Gundersen, 2008). Whether and how the cytoskeleton determines the polar reaction of cells upon directional shear stress application still needs to be elucidated.

Limitations of the Study

In current system, a classic cell line, HeLa cell, is chosen to observe heterogeneous distribution of membrane tension in response to shear stress. It is reported that the direction of cell migration in tumor cells is opposite to that in endothelial cells, indicating that there may be entirely different mechanotransduction pathways in these two kinds of cell lines. Therefore, some different results probably can be achieved by using vascular endothelial cells instead of HeLa cells.

METHODS

All methods can be found in the accompanying Transparent Methods supplemental file.

SUPPLEMENTAL INFORMATION

Supplemental Information includes Transparent Methods, 3 figures, 2 tables, and 10 videos and can be found with this article online at https://doi.org/10.1016/j.isci.2018.09.002.

ACKNOWLEDGMENTS

We thank J. Sun and S. Zhang at the State Key Laboratory of Brain and Cognitive Sciences for plasmid construction and helpful discussion. The study was financially supported by the NSFC (No. 31670867, 31670961).

AUTHOR CONTRIBUTIONS

B.L. and X.L. designed and supervised the project. W.L. and X.Y. performed experiments and analyzed the data. F.X., B.Z., S.S., and C.G. analyzed the data. W.L. and A.u.R.A. wrote the manuscript. All authors proofread the manuscript and provided comments.

DECLARATION OF INTERESTS

The authors declare no competing interests.

Received: April 23, 2018
Revised: July 10, 2018
Accepted: September 3, 2018
Published: September 28, 2018

REFERENCES

Alenghat, F.J., and Ingber, D.E. (2002). Mechanotransduction: all signals point to cytoskeleton, matrix, and integrins. Sci. STKE *2002*, pe6.

Allen, J.A., Halverson-Tamboli, R.A., and Rasenick, M.M. (2007). Lipid raft microdomains and neurotransmitter signalling. Nat. Rev. Neurosci. *8*, 128–140.

Altman, G.H., Horan, R.L., Martin, I., Farhadi, J., Stark, P.R., Volloch, V., Richmond, J.C., Vunjak-Novakovic, G., and Kaplan, D.L. (2002). Cell differentiation by mechanical stress. FASEB J. *16*, 270–272.

Apodaca, G. (2002). Modulation of membrane traffic by mechanical stimuli. Am. J. Physiol. Renal Physiol. *282*, F179–F190.

Boycott, H.E., Barbier, C.S., Eichel, C.A., Costa, K.D., Martins, R.P., Louault, F., Dilanian, G., Coulombe, A., Hatem, S.N., and Balse, E. (2013). Shear stress triggers insertion of voltage-gated potassium channels from intracellular compartments in atrial myocytes. Proc. Natl. Acad. Sci. USA *110*, E3955–E3964.

Butler, P.J., Norwich, G., Weinbaum, S., and Chien, S. (2001). Shear stress induces a time- and position-dependent increase in endothelial cell membrane fluidity. Am. J. Physiol. Cell Physiol. *280*, C962–C969.

Butler, P.J., Tsou, T.C., Li, J.Y., Usami, S., and Chien, S. (2002). Rate sensitivity of shear-induced changes in the lateral diffusion of endothelial cell membrane lipids: a role for membrane perturbation in shear-induced MAPK activation. FASEB J. *16*, 216–218.

Chachisvilis, M., Zhang, Y.L., and Frangos, J.A. (2006). G protein-coupled receptors sense fluid shear stress in endothelial cells. Proc. Natl. Acad. Sci. USA *103*, 15463–15468.

Chichili, G.R., and Rodgers, W. (2009). Cytoskeleton-membrane interactions in membrane raft structure. Cell. Mol. Life Sci. *66*, 2319–2328.

Choi, C.K., and Helmke, B.P. (2008). Short-term shear stress induces rapid actin dynamics in living endothelial cells. Mol. Cell. Biomech. *5*, 247–258.

Cramer, L.P. (1999). Organization and polarity of actin filament networks in cells: implications for the mechanism of myosin-based cell motility. Biochem. Soc. Symp. *65*, 173–205.

Dai, J., and Sheetz, M.P. (1999). Membrane tether formation from blebbing cells. Biophys. J. *77*, 3363–3370.

Davies, P.F. (2009). Hemodynamic shear stress and the endothelium in cardiovascular pathophysiology. Nat. Clin. Pract. Cardiovasc. Med. *6*, 16–26.

Diz-Munoz, A., Fletcher, D.A., and Weiner, O.D. (2013). Use the force: membrane tension as an organizer of cell shape and motility. Trends Cell Biol. *23*, 47–53.

Freikamp, A., Mehlich, A., Klingner, C., and Grashoff, C. (2017). Investigating piconewton

forces in cells by FRET-based molecular force microscopy. J. Struct. Biol. *197*, 37–42.

Galbraith, C.G., Skalak, R., and Chien, S. (1998). Shear stress induces spatial reorganization of the endothelial cell cytoskeleton. Cell Motil. Cytoskeleton *40*, 317–330.

Gauthier, N.C., Fardin, M.A., Roca-Cusachs, P., and Sheetz, M.P. (2011). Temporary increase in plasma membrane tension coordinates the activation of exocytosis and contraction during cell spreading. Proc. Natl. Acad. Sci. USA *108*, 14467–14472.

Gauthier, N.C., Rossier, O.M., Mathur, A., Hone, J.C., and Sheetz, M.P. (2009). Plasma membrane area increases with spread area by exocytosis of a GPI-anchored protein compartment. Mol. Biol. Cell *20*, 3261–3272.

Goldfinger, L.E., Tzima, E., Stockton, R., Kiosses, W.B., Kinbara, K., Tkachenko, E., Gutierrez, E., Groisman, A., Nguyen, P., Chien, S., et al. (2008). Localized alpha4 integrin phosphorylation directs shear stress-induced endothelial cell alignment. Circ. Res. *103*, 177–185.

Grashoff, C., Hoffman, B.D., Brenner, M.D., Zhou, R., Parsons, M., Yang, M.T., McLean, M.A., Sligar, S.G., Chen, C.S., Ha, T., et al. (2010). Measuring mechanical tension across vinculin reveals regulation of focal adhesion dynamics. Nature *466*, 263–266.

Guevorkian, K., Manzi, J., Pontani, L.L., Brochard-Wyart, F., and Sykes, C. (2015). Mechanics of biomimetic liposomes encapsulating an actin shell. Biophys. J. *109*, 2471–2479.

Guo, J., Sachs, F., and Meng, F. (2014). Fluorescence-based force/tension sensors: a novel tool to visualize mechanical forces in structural proteins in live cells. Antioxid. Redox Signal. *20*, 986–999.

Hall, A. (1998). Rho GTPases and the actin cytoskeleton. Science *279*, 509–514.

Hochmuth, R.M. (2000). Micropipette aspiration of living cells. J. Biomech. *33*, 15–22.

Houk, A.R., Jilkine, A., Mejean, C.O., Boltyanskiy, R., Dufresne, E.R., Angenent, S.B., Altschuler, S.J., Wu, L.F., and Weiner, O.D. (2012). Membrane tension maintains cell polarity by confining signals to the leading edge during neutrophil migration. Cell *148*, 175–188.

Keren, K. (2011). Membrane tension leads the way. Proc. Natl. Acad. Sci. USA *108*, 14379–14380.

Kim, M., Song, K., Jin, E.J., and Sonn, J. (2012). Staurosporine and cytochalasin D induce chondrogenesis by regulation of actin dynamics in different way. Exp. Mol. Med. *44*, 521–528.

Kozlov, M.M., and Chernomordik, L.V. (2015). Membrane tension and membrane fusion. Curr. Opin. Struct. Biol. *33*, 61–67.

Kuchnir Fygenson, D., Elbaum, M., Shraiman, B., and Libchaber, A. (1997). Microtubules and vesicles under controlled tension. Phys. Rev. E Stat. Phys. Plasmas Fluids Relat. Interdiscip. Topics *55*, 850–859.

Lafaurie-Janvore, J., Maiuri, P., Wang, I., Pinot, M., Manneville, J.B., Betz, T., Balland, M., and Piel, M. (2013). ESCRT-III assembly and cytokinetic abscission are induced by tension release in the intercellular bridge. Science *339*, 1625–1629.

Li, R., and Gundersen, G.G. (2008). Beyond polymer polarity: how the cytoskeleton builds a polarized cell. Nat. Rev. Mol. Cell Biol. *9*, 860–873.

Lieber, A.D., Yehudai-Resheff, S., Barnhart, E.L., Theriot, J.A., and Keren, K. (2013). Membrane tension in rapidly moving cells is determined by cytoskeletal forces. Curr. Biol. *23*, 1409–1417.

Liu, B., Kim, T.J., and Wang, Y. (2010). Live cell imaging of mechanotransduction. J. R. Soc. Interface *7 Suppl 3*, S365–S375.

Liu, B., Lu, S., Hu, Y.L., Liao, X., Ouyang, M., and Wang, Y. (2014). RhoA and membrane fluidity mediates the spatially polarized Src/FAK activation in response to shear stress. Sci. Rep. *4*, 7008.

Liu, B., Lu, S., Zheng, S., Jiang, Z., and Wang, Y. (2011). Two distinct phases of calcium signalling under flow. Cardiovasc. Res. *91*, 124–133.

Liu, Y., Galior, K., Ma, V.P., and Salaita, K. (2017). Molecular tension probes for imaging forces at the cell surface. Acc. Chem. Res. *50*, 2915–2924.

McCue, S., Dajnowiec, D., Xu, F., Zhang, M., Jackson, M.R., and Langille, B.L. (2006). Shear stress regulates forward and reverse planar cell polarity of vascular endothelium in vivo and in vitro. Circ. Res. *98*, 939–946.

McGarry, J.G., Klein-Nulend, J., Mullender, M.G., and Prendergast, P.J. (2005). A comparison of strain and fluid shear stress in stimulating bone cell responses–a computational and experimental study. FASEB J. *19*, 482–484.

Mitchell, M.J., and King, M.R. (2013). Computational and experimental models of cancer cell response to fluid shear stress. Front. Oncol. *3*, 44.

Morimatsu, M., Mekhdjian, A.H., Adhikari, A.S., and Dunn, A.R. (2013). Molecular tension sensors report forces generated by single integrin molecules in living cells. Nano Lett. *13*, 3985–3989.

Na, S., Collin, O., Chowdhury, F., Tay, B., Ouyang, M., Wang, Y., and Wang, N. (2008). Rapid signal transduction in living cells is a unique feature of mechanotransduction. Proc. Natl. Acad. Sci. USA *105*, 6626–6631.

Pfafferott, C., Nash, G.B., and Meiselman, H.J. (1985). Red blood cell deformation in shear flow. effects of internal and external phase viscosity and of in vivo aging. Biophys. J. *47*, 695–704.

Poh, Y.C., Na, S., Chowdhury, F., Ouyang, M., Wang, Y., and Wang, N. (2009). Rapid activation of Rac GTPase in living cells by force is independent of Src. PLoS One *4*, e7886.

Raucher, D., and Sheetz, M.P. (2000). Cell spreading and lamellipodial extension rate is regulated by membrane tension. J. Cell Biol. *148*, 127–136.

Raucher, D., Stauffer, T., Chen, W., Shen, K., Guo, S., York, J.D., Sheetz, M.P., and Meyer, T. (2000). Phosphatidylinositol 4,5-bisphosphate functions as a second messenger that regulates cytoskeleton-plasma membrane adhesion. Cell *100*, 221–228.

Rouven Bruckner, B., Pietuch, A., Nehls, S., Rother, J., and Janshoff, A. (2015). Ezrin is a major regulator of membrane tension in epithelial cells. Sci. Rep. *5*, 14700.

Sechi, A.S., and Wehland, J. (2000). The actin cytoskeleton and plasma membrane connection: PtdIns(4,5)P(2) influences cytoskeletal protein activity at the plasma membrane. J. Cell Sci. *113 Pt 21*, 3685–3695.

Shao, S., Xiang, C., Qin, K., Ur Rehman Aziz, A., Liao, X., and Liu, B. (2017). Visualizing the spatiotemporal map of Rac activation in bovine aortic endothelial cells under laminar and disturbed flows. PLoS One *12*, e0189088.

Smith, A.S., Nowak, R.B., Zhou, S., Gianetto, M., Gokhin, D.S., Papoin, J., Ghiran, I.C., Blanc, L., Wan, J., and Fowler, V.M. (2017). Myosin IIA interacts with the spectrin-actin membrane skeleton to control red blood cell membrane curvature and deformability. Proc. Natl. Acad. Sci. USA *115*, E4377–E4385.

Stabley, D.R., Jurchenko, C., Marshall, S.S., and Salaita, K.S. (2011). Visualizing mechanical tension across membrane receptors with a fluorescent sensor. Nat. Methods *9*, 64–67.

Tinevez, J.Y., Schulze, U., Salbreux, G., Roensch, J., Joanny, J.F., and Paluch, E. (2009). Role of cortical tension in bleb growth. Proc. Natl. Acad. Sci. USA *106*, 18581–18586.

Togo, T., Krasieva, T.B., and Steinhardt, R.A. (2000). A decrease in membrane tension precedes successful cell-membrane repair. Mol. Biol. Cell *11*, 4339–4346.

Tzima, E., Kiosses, W.B., del Pozo, M.A., and Schwartz, M.A. (2003). Localized cdc42 activation, detected using a novel assay, mediates microtubule organizing center positioning in endothelial cells in response to fluid shear stress. J. Biol. Chem. *278*, 31020–31023.

Viola, A., and Gupta, N. (2007). Tether and trap: regulation of membrane-raft dynamics by actin-binding proteins. Nat. Rev. Immunol. *7*, 889–896.

Wan, Q., Kim, S.J., Yokota, H., and Na, S. (2013). Differential activation and inhibition of RhoA by fluid flow induced shear stress in chondrocytes. Cell Biol. Int. *37*, 568–576.

Xie, T., Hawkins, J., and Sun, Y. (2017). Traction force measurement using deformable microposts. Methods Mol. Biol. *1627*, 235–244.

Zaal, K.J., Reid, E., Mousavi, K., Zhang, T., Mehta, A., Bugnard, E., Sartorelli, V., and Ralston, E. (2011). Who needs microtubules? myogenic reorganization of MTOC, Golgi complex and ER exit sites persists despite lack of normal microtubule tracks. PLoS One *6*, e29057.

ISCI, Volume *7*

Supplemental Information

A Membrane-Bound Biosensor Visualizes Shear Stress-Induced Inhomogeneous Alteration of Cell Membrane Tension

Wang Li, Xinlei Yu, Fei Xie, Baohong Zhang, Shuai Shao, Chunyang Geng, Aziz ur Rehman Aziz, Xiaoling Liao, and Bo Liu

Supplemental information

Supplemental Figures

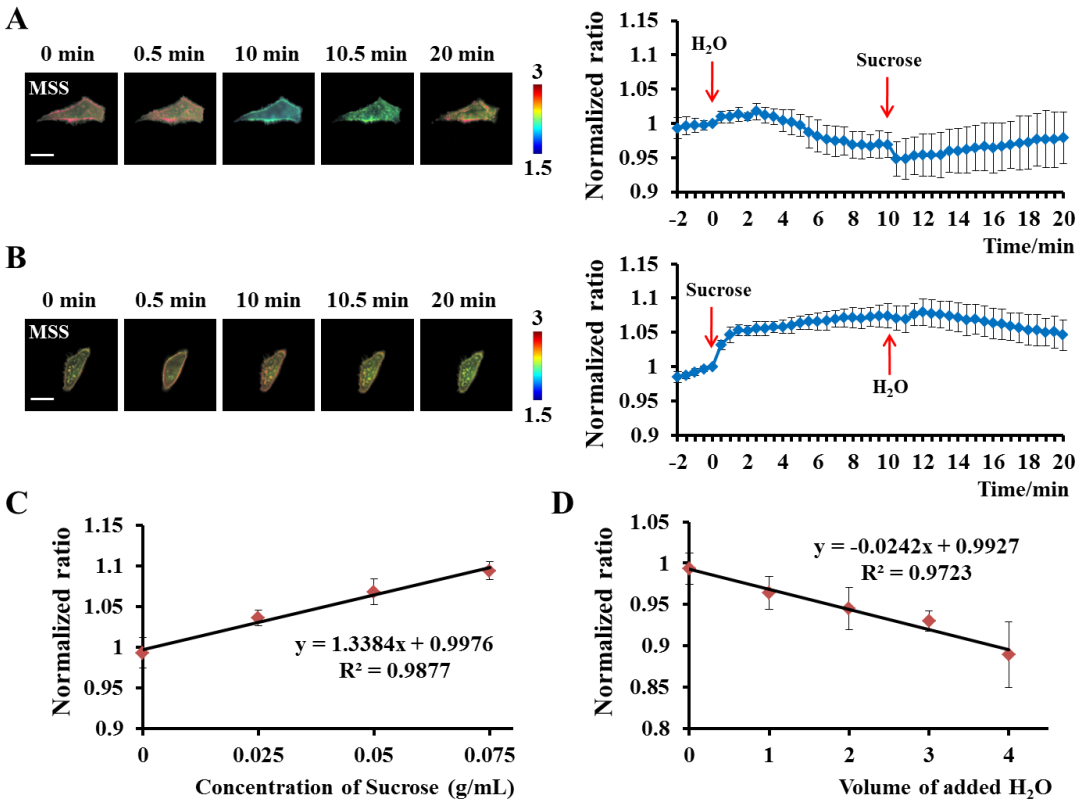

Figure S1. The response of MSS biosensor is reversible and linear to the changes in membrane tension. Related to Figure 1. (A) The representative YPet/ECFP emission ratio images and their average time courses of MSS in HeLa cells after exposure to hypotonic solution at 0 min then to hypertonic solution at 10 min (n = 5). (B) The representative YPet/ECFP emission ratio images and their average time courses of MSS in HeLa cells after exposure to hypertonic solution at 0 min then to hypotonic solution at 10 min (n = 5). (C) Normalized YPet/ECFP emission ratio of MSS exposed to different concentrations of sucrose solution or (D) to hypotonic solution by adding different volumes of H_2O. All error bars represent S.E.M. Scale bar, 20 μm.

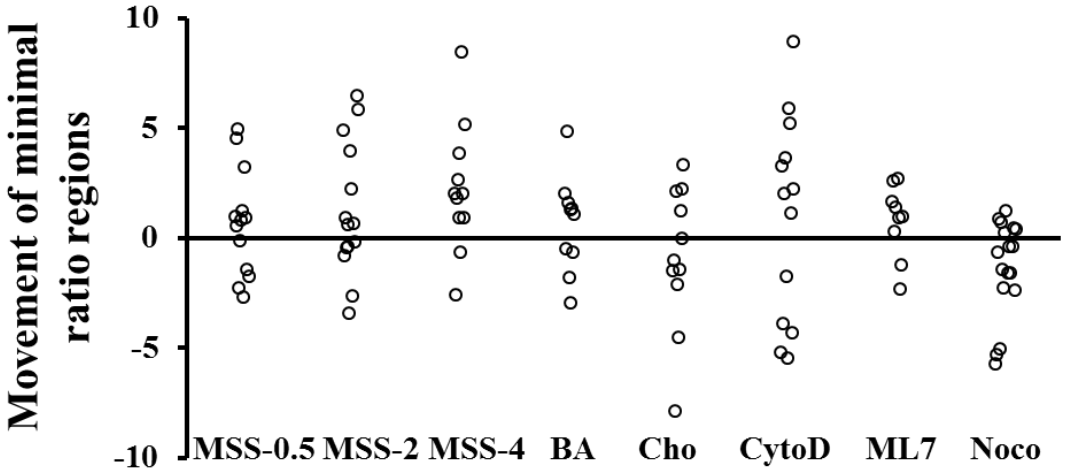

Figure S2. Movement of minimal ratio regions after 15 min of shear stress application. Related to Figures 3, 5 and 7. Positive value means the minimal ratio region moves toward downstream.

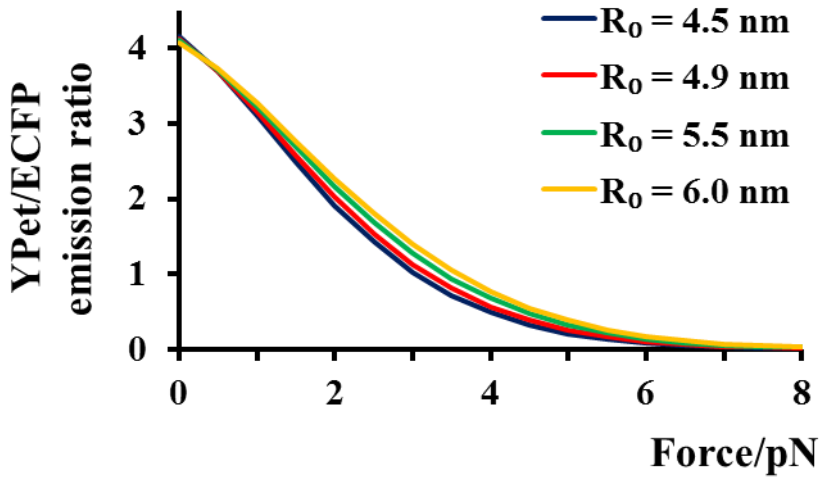

Figure S3. YPet/ECFP emission ratio versus force calibration curves calculated with Förster radius ranging from 4.5 to 6.0 nm. Related to Figures 3, 5 and 7. R_0 = 4.9 nm is used for estimating the relationship between emission ratio and force in present study. Variation in Förster radius causes gently perturbation to the calibration curves.

Table S1. The parameters from initial fitting curve in different groups. Related to Figures 3, 5 and 7.

	y0+A	xc	y (x=1)	y (x=50)
MSS-0.5	3.5054±0.6774	24.4885±5.3548	4.2956±0.7563*	4.4022±0.7193*
MSS-2	3.1864±0.8771	27.1474±4.6017	3.5487±1.0198	3.5680±1.0461
MSS-4	2.5756±0.6298	27.8589±5.1138	3.1843±0.7613	3.1890±0.8992
Benzyl alcohol	2.7525±0.3410	21.8215±4.9650*	3.1660±0.5139	3.2973±0.3774
Cholesterol	1.5633±0.3153*	21.1635±3.8434*	1.7539±0.3689*	1.8002±0.3671*
Cytochalasin D	2.6067±0.5252*	25.6323±5.5785	2.9345±0.6824	2.9558±0.6171
ML7	2.7966±0.6833	28.1219±5.6882	3.2052±0.8726	3.2148±0.9122
Nocodazole	2.8693±0.4770	24.514±5.7095	3.1732±0.6060	3.2514±0.5804

Table S2. The parameters from last fitting curve in different groups. Related to Figures 3, 5 and 7.

	y0+A	xc	y (x=1)	y (x=50)
MSS-0.5	2.5748±0.4882	23.8299±5.2256	2.9726±0.5380	3.1001±0.5445
MSS-2	2.6915±0.7536	25.9075±3.7722	2.9823±0.8749	3.0253±0.8709
MSS-4	1.9347±0.4133*	25.6458±4.3844	2.2230±0.4946*	2.2731±0.5593*
Benzyl alcohol	1.8641±0.1806*	21.2209±5.4675*	2.0052±0.2333*	2.0743±0.1810*
Cholesterol	1.3986±0.2444*	22.0506±4.8602*	1.5483±0.2979*	1.5897±0.3102*
Cytochalasin D	1.9663±0.3698*	24.7602±3.8503	2.2192±0.4928*	2.2479±0.4817*
ML7	2.1628±0.4167*	26.4341±6.0281	2.4664±0.5416	2.4710±0.5577
Nocodazole	2.7854±0.4575	25.8838±5.9417	3.1133±0.5633	3.1479±0.5326

*P<0.05 compared with MSS-2 group

Transparent Methods

Gene construction and DNA plasmids

An elastic linker of tension sensor module is derived from the spider silk protein flagelliform in which amino acid is $(GPGGA)_8$ (Grashoff et al., 2010). The DNA sequence of linker is changed to a series of nonredundant sequence (shown below) by utilizing the degeneracy of codon in order to overcome the difficulties in constructing objective plasmids.

5'-GGTCCAGGAGGCGCAGGACCTGGCGGGGCTGGACCGGGTGGCGCGGGACCCGGC GGAGCCGGCCCAGGTGGGGCGGGCCCTGGTGGTGCTGGTCCGGGAGGGGCAGGGCCCGG AGGTGCC-3'

The linker sequences are added to C-terminal of YPet through polymerase chain reaction (PCR). After that, the PCR products are fused with an N-terminal ECFP to attain the tension sensor module. The membrane-bound tension biosensor, MSS, is constructed by PCR with a forward primer containing 21 amino acids from Lyn kinase and a reverse primer containing 14 amino acids from K-Ras (Pyenta et al., 2001; Hancock, 2003), which can link the tension sensor to phospholipids in the region of lipid raft and non-lipid raft, respectively (Andrisani et al., 2015; Niv et al., 2002). Control sensor (KMSS) is a head-less mutant, which is constructed by PCR amplification from MSS without the Lyn part. All the constructs are cloned into pcDNA3.1 (+) for mammalian cells expression.

Flow system

Flow system is a circulation loop system including a dynamic device (peristaltic pump), a parallel-plate flow chamber and an observation system as previously described (Liu et al., 2014). Cells seeded on the glass slide are exposed to shear stress, which can be calculated as equation (1):

$$\tau = \frac{6\mu Q}{bh^2} \tag{1}$$

Here τ = fluid shear stress (Pa), μ = fluid viscosity of solution (cp), Q = flow rate (cm^3/s), b = width (mm), h = height (mm). In this experiment, μ = 0.82 cp (dulbecco's modified eagle medium (DMEM) containing 0.5% fetal bovine serum (FBS)), b = 13 mm, h = 0.508 mm. By adjusting fluid flow in the chamber, laminar shear stress is set as 0.5, 2 and 4 Pa, respectively. The conditions of the flow experiments are maintained at 37 ℃ and pH 7.4 with 5% CO_2.

Cell culture and transfection

HeLa cells (ATCC) are cultured in DMEM (Gibco) containing 10% FBS (Hyclone), 100 unit/ml penicillin and 100 μg/ml streptomycin in a humidified incubator of 95% O_2 and 5% CO_2 at 37 ˚C. The DNA plasmids are transected into cells by using Lipofectamine 3000 reagent (Invitrogen) according to the company protocol.

Microscope, image acquisition and analysis

An inverted fluorescence microscope (Nikon Eclipse Ti Se-ries, Ti-Fl Epi-fl/1) equipped with a cooled charge-coupled device (CCD) camera (Evolve^{TM}512, Photometrics) is used in this experiment, as well as a 420DF20 excitation filter, a 455DRLP dichroic mirror and two emission filters controlled by a filter controller (480DF30 for CFP and 535DF25 for YFP). All the images are acquired according to the methods as described previously by using MetaFluor 6.2 software (Universal Imaging) with an interval of 30 seconds for each shoot on a single cell (Liu et al., 2014). FRET ratio images are formed by calculating YPet / ECFP, and mean ratio of the whole cell at each time step is obtained simultaneously. After that, a time-dependent change of ratio is generated to describe the overall changes of membrane tension.

To quantify the distribution of membrane tension, a MATLAB (Mathworks; Natick, MA) software package is developed to process fluorescent images. After loading the images to be processed, the background is subtracted considering the average of fluorescence intensity in 4 corners of images as baseline. Next median filter and morphological close operation are applied to remove noise in images, followed by cell boundary identification. After that, the isolated cell is divided into 50 sections equally along the direction of shear stress in which FRET ratio is presumed to be the same as previously described (Shao et al., 2017). Upstream represents cellular edge facing to shear stress while downstream represents the other cellular terminals. These 50 sections are numbered as 1 to 50 in which 1 represents the last part of downstream while 50 represents the first part of upstream. Thus a three-dimensional diagram is obtained to describe the changes of FRET ratio in every region with time.

To obtain the local changes of FRET ratio for detail, an Extreme equation (shown in (2) and (3)) is adopted to fit the data at time 0 and 15 min respectively, with the help of 1stOpt software (7D-Soft High Technology Inc.).

$$y = y0 + A \times e^{(-e^{-z} - z + 1)} \tag{2}$$

$$z = (x - xc) / w \tag{3}$$

These equations describe a curve with an extreme point of (xc, y0+A). And in the current experiment, (y0+A) stands for the minimum FRET ratio while xc for its position. Since the fitting curve decreases monotonously first and then increases later, x is set as 1 or 50 to get the maximum FRET ratio of downstream or upstream according to Extreme equation, respectively. Therefore, some parameters can be calculated as below (All the normalizations are based on time 0.):

Normalized minimum FRET ratio = the minimum FRET ratio at time 15 min / the minimum FRET ratio at time 0,

Movement of minimum FRET ratio = Position of minimum FRET ratio at time 0 – Position of minimum FRET ratio at time 15 min,

U = the maximum FRET ratio of upstream – the minimum FRET ratio,

D = the maximum FRET ratio of downstream – the minimum FRET ratio,

Upstream variation range (UVR) = U value at time 15 min / U value at time 0,

Downstream variation range (DVR) = D value at time 15 min / D value at time 0.

FRET ratio to force calculation

FRET efficiency E can be calculated by equation (4) as previous reports (Morimatsu et al., 2013).

$$E = \frac{E_{transfer}}{E_{total}} \tag{4}$$

$E_{transfer}$ = the energy transferred from the donor, and E_{total} = the total energy of the donor.

In present study, $E_{transfer}$ = the energy of YPet, E_{total} = the total energy of ECFP and YPet. Hence, FRET efficiency can also be calculated as equation (5) where YPet / ECFP emission ratio ER = E_{YPet} / E_{ECFP}.

$$E = \frac{E_{YPet}}{E_{ECFP} + E_{YPet}} = \frac{1}{\frac{1}{ER} + 1} \tag{5}$$

Based on the standard FRET equation (6), in which R = the distance between donor and acceptor, and R_0 = the donor-acceptor distance at which 50% FRET occurs, termed Förster radius, the FRET vs

force calibration for the current spring linker $(GPGGA)_8$ domain as previous reports, can be converted to a force-extension curve R(f) (Grashoff et al., 2010).

$$E = \frac{1}{1+(R/R_0)^6} \quad (6)$$

Then the force-dependent donor-acceptor distance in the MSS is calculated as previously described (equation (7)) (Morimatsu et al., 2013).

$$R = R_{MSS} - R_{TSMod} + R(f) \quad (7)$$

R_{MSS} represents the no-load donor-acceptor distance of MSS biosensor. R_0 = 4.9 nm for ECFP and EYFP can be considered to be an approximate reference for our FRET pair (Bajar et al., 2016). By using R_0 of 4.9 nm, equation (5) and (6), R_{MSS} is calculated to be 3.99 nm as the measured no-load FRET ratio is 3.86. The resting length of TSMod R_{TSMod} is 7.3 nm based on the no-load FRET efficiency of ~23.5% (Grashoff et al., 2010). Therefore, the distance vs force curve for MSS can be converted to FRET ratio vs force by using equation (5), (6) and (7). Then these resultant data points are fitted by fourth order polynomial to provide a intuitive relation between FRET ratio and force.

Statistical analysis

The number of independent experiments (n) is indicated in the figure legends. All the statistical difference analyses between groups are measured by unpaired, two-tailed Student's t-Test function of Excel software (Microsoft). A significant difference is determined by P value ($P < 0.05$).

Supplemental References

Andrisani, A., Dona, G., Tibaldi, E., Brunati, A.M., Sabbadin, C., Armanini, D., Alvisi, G., Gizzo, S., Ambrosini, G., Ragazzi, E., *et al.* (2015). Astaxanthin Improves Human Sperm Capacitation by Inducing Lyn Displacement and Activation. Mar. Drugs *13*, 5533-5551.

Bajar, B.T., Wang, E.S., Zhang, S., Lin, M.Z., and Chu, J. (2016). A Guide to Fluorescent Protein FRET Pairs. Sensors (Basel, Switzerland) *16*.

Grashoff, C., Hoffman, B.D., Brenner, M.D., Zhou, R., Parsons, M., Yang, M.T., McLean, M.A., Sligar, S.G., Chen, C.S., Ha, T., *et al.* (2010). Measuring mechanical tension across vinculin reveals regulation of focal adhesion dynamics. Nature *466*, 263-266.

Hancock, J.F. (2003). Ras proteins: different signals from different locations. Nat. Rev. Mol. Cell Biol. *4*, 373-384.

Liu, B., Lu, S., Hu, Y.L., Liao, X., Ouyang, M., and Wang, Y. (2014). RhoA and membrane fluidity mediates the spatially polarized Src/FAK activation in response to shear stress. Sci. Rep. *4*, 7008.

Morimatsu, M., Mekhdjian, A.H., Adhikari, A.S., and Dunn, A.R. (2013). Molecular tension sensors report forces generated by single integrin molecules in living cells. Nano Lett. *13*, 3985-3989.

Niv, H., Gutman, O., Kloog, Y., and Henis, Y.I. (2002). Activated K-Ras and H-Ras display different interactions with saturable nonraft sites at the surface of live cells. J Cell Biol *157*, 865-872.

Pyenta, P.S., Holowka, D., and Baird, B. (2001). Cross-correlation analysis of inner-leaflet-anchored green fluorescent protein co-redistributed with IgE receptors and outer leaflet lipid raft components. Biophys J *80*, 2120-2132.

Shao, S., Xiang, C., Qin, K., Ur Rehman Aziz, A., Liao, X., and Liu, B. (2017). Visualizing the spatiotemporal map of Rac activation in bovine aortic endothelial cells under laminar and disturbed flows. PLoS One *12*, e0189088.